Comparison of the early stages of forced unfolding for fibronectin type III modules

David Craig*, André Krammer*†, Klaus Schulten‡, and Viola Vogel*‡§

*Department of Bioengineering, University of Washington, Seattle, WA 98195; and ‡Beckman Institute, University of Illinois, 405 North Mathews Avenue, Urbana, IL 61801

Edited by Jiri Jonas, University of Illinois, Urbana, IL, and approved February 26, 2001 (received for review December 7, 2000)

The structural changes accompanying stretch-induced early unfolding events were investigated for the four type III fibronectin (FN-III) modules, FN-III$_7$, FN-III$_8$, FN-III$_9$, and FN-III$_{10}$ by using steered molecular dynamics. Simulations revealed that two main energy barriers, I and II, have to be overcome to initiate unraveling of FN-III's tertiary structure. In crossing the first barrier, the two opposing β-sheets of FN-III are rotated against each other such that the β-strands of both β-sheets align parallel to the force vector (aligned state). All further events in the unfolding pathway proceed from this intermediate state. A second energy barrier has to be overcome to break the first major cluster of hydrogen bonds between adjacent β-strands. Simulations revealed that the height of barrier I varied significantly among the four modules studied, being largest for FN-III$_7$ and lowest for FN-III$_{10}$, whereas the height of barrier II showed little variation. Key residues affecting the mechanical stability of FN-III modules were identified. These results suggest that FN-III modules can be prestretched into an intermediate state with only minor changes to their tertiary structures. FN-III$_{10}$, for example, extends 12 Å from the native ''twisted'' to the intermediate aligned state, and an additional 10 Å from the aligned state to further unfolding where the first β-strand is peeled away. The implications of the existence of intermediate states regarding the elasticity of fibrillar fibers and the stretch-induced exposure of cryptic sites are discussed.

The mechanical properties of fibronectin (FN) and its extracellular matrix fibers have drawn considerable attention recently. FN is a 450- to 500-kDa dimeric protein composed of more than 20 modules per monomer. FN primarily consists of three structurally homologous modules, FN-I, FN-II, and FN-III, presented schematically in Fig. 1*A*. Cells assemble FN into fibrillar networks that provide mechanical stability to the extracellular matrix and connective tissue. Furthermore, cells have been found to mechanically stretch FN fibers by up to four times their normal length (1). This wide extension range is attributed to the unfolding of individual FN modules under tension, which are presumed to refold when tension is released (2, 3). The FN-III modules are of particular interest because they contain several cell recognition sites, including the synergy site on FN-III$_9$ and an RGD loop on FN-III$_{10}$ (4). Beyond its role in FN, the FN-III motif is structurally ubiquitous and found in 2% of all animal proteins (5). The FN-III motif is a Greek key β-sandwich (Fig. 1*B*) with four β-strands in the upper sheet and three in the lower sheet (6).

Mechanical forces, in addition to chemical cues, have been implicated in playing a critical role in regulating the functional states of FN. Binding sites buried within the protein in its native state, also referred to as cryptic sites, can be exposed by denaturation, or potentially through mechanical stretching (7, 8). Forced unfolding of the FN-III$_{10}$ module also has been suggested to modify exposure of the RGD loop, thus influencing FN′s accessibility to integrins (9). Mechanical forces, furthermore, are essential in initiating FN fibril assembly (10), potentially through exposure of cryptic sites, and/or by swapping complementary β-strands of partially unfolded FN-III modules during refolding (11, 12). The functional states of FN are tightly regulated because FN is central in mediating and regulating cell adhesion, proliferation, and migration through various integrin-dependent signaling pathways (5).

The effect of mechanical force on FN-III and homologous modules has been studied by using atomic force microscopy (AFM) (13–15) and optical tweezers (16). Forced unfolding of modular proteins often exhibits a saw-tooth pattern when the applied external force is plotted vs. the extension of the protein. Each major force peak coincides with the rupturing of tertiary structure for one of its modules. For the muscle protein titin, AFM experiments have further shown that homologous β-sandwich motifs can exhibit different relative maximal forces in force extension curves, and hence may vary significantly in their mechanical stability against stretching (17, 18). Although AFM and optical tweezers have provided information on the forces required for the sequential rupture of modules, these methods cannot provide structural insights into how the modules are ruptured and whether there are critical force bearing interactions that control mechanical stability.

To learn how mechanical forces change the structure of modular proteins and their functional states, one must derive an atomic level picture of the stretching process. In our study, we use steered molecular dynamics (SMD) simulations to deduce structural insight into early events in the forced unfolding pathway of different FN-III modules and to compare their relative mechanical stability. Starting with a known crystal structure of single modules equilibrated with explicit water, the structural changes are simulated as the proteins are unfolded under constant force (cf-SMD) or are pulled apart under constant velocity (cv-SMD) conditions mimicking AFM experiments. SMD studies of the forced unfolding of single modules of titin (I27) reproduced the existence of a major force peak in force extension curves (19). SMD simulations, furthermore, predicted correctly the relative mechanical stabilities of titin I27 and I28 that were later verified by AFM measurements (18). Another validation of the SMD method is the identification of the major force-bearing residues in titin modules I27 and I28, which have been proven correct by point mutations of I27 (20).

The force-induced rupturing of FN-III modules and associated structural changes have been studied previously by AFM (14, 15, 17) as well as by SMD (9, 21) and a related computational method (22, 23). Previous computation studies primarily have focused on describing the peeling away of the first β-strands. Our analysis presented here focuses on the early events in the stretching of the four human FN-III modules, FN-III$_7$, FN-III$_8$, FN-III$_9$, and FN-III$_{10}$, for extensions of less than ≈30 Å. We address whether stretching of these four FN-III modules pro-

This paper was submitted directly (Track II) to the PNAS office.

Abbreviations: SMD, steered molecular dynamics; cf-SMD, constant force SMD; cv-SMD, constant velocity SMD; FN, fibronectin; AFM, atomic force microscopy.

†Present address: Molecular Simulations Inc., 9685 Scranton Road, San Diego, CA 92121.

§To whom reprint requests should be addressed. E-mail: vvogel@u.washington.edu.

The publication costs of this article were defrayed in part by page charge payment. This article must therefore be hereby marked "*advertisement*" in accordance with 18 U.S.C. §1734 solely to indicate this fact.

 www.pnas.org/cgi/doi/10.1073/pnas.101582198

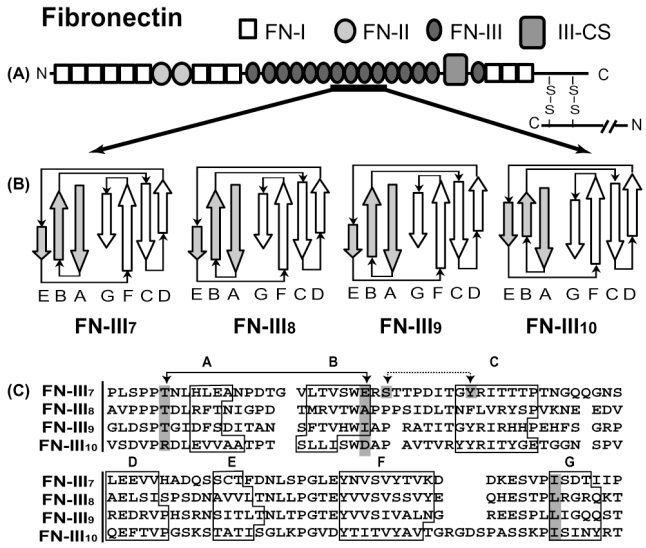

Fig. 1. Structure of the human FN monomer. (*A*) Modular structure of FN protein emphasizing folding motifs, FN-I, FN-II, and FN-III. (*B*) Secondary structures of selected FN-III modules with accurate representations of relative β-strand lengths with respect to each other. The upper sheets are shaded gray while lower sheets are white. (*C*) Sequence alignment of the four FN-III modules. FN-III$_7$, FN-III$_8$, FN-III$_9$, and FN-III$_{10}$ have 93, 91, 91, and 94 aa, respectively. Key residues discussed within the text are highlighted in dark gray, while residues forming key hydrogen bonds are connected by arrows.

ceeds along identical pathways and whether intermediate states exist between their native state and the state when the first β-strand peels away from the protein. We further provide comparisons between the relative potential energy barrier heights that must be overcome to stretch FN-III modules. Finally, we describe key structure and sequence differences between these four FN-III modules that appear to have a major impact on their mechanical stability. Knowledge about the relative mechanical stability of four of over 15 homologous FN-III modules will provide further insight into how structure and sequence leads to mechanical stability and how this in turn may relate to function.

Methods

Single FN-III modules were adopted from the x-ray crystallographic structure of the tetramer FN-III$_{7–10}$ (Protein DataBank code 1FNF) (4). Molecular dynamics simulations were carried out in an explicit all-atom model with the CHARMM22 force field (24) and TIP3P (25) water parameters using the programs NAMD (26) and X-PLOR (27). All simulations were performed with a time step of 1 fs, a uniform dielectric constant of 1, and a cutoff of nonbonded forces with a switching function starting at a distance of 10 Å and reaching zero at 13 Å. Solvation and thermalization of single FN-III modules were modeled as described in previous studies (9, 19). Modules were solvated in a sphere of explicit water molecules with a radius of 32 Å, resulting in ≈13,000 atoms. Systems were minimized for 2,000 steps and then thermalized to 300 K over 30 ps in 30 K temperature increments using X-PLOR (27). Finally, the hydrated modules were equilibrated for a total of 60 ps: during the first 20 ps, the modules were coupled to an external heat bath with harmonic restraints on the outer 3-Å shell of water, coupling to the heat bath was eliminated during the following 20 ps; during the final 20 ps the harmonic restraints were also eliminated. Equilibrating for an additional 20, 40, and 60 ps generated starting additional starting structures from equilibrium. These additional structures were used as controls when multiple simulations were conducted with the same stretching force applied to the module.

Table 1. Comparison of end-to-end distances of the four FN-III modules, and the midpoint extensions for the first and second plateaus obtained from the extension time curves

Module	End-to-end distance (Å), equilibrated structure	Force induced extension (Å) from equilibrated structure	
		Twisted state	Aligned state
FN-III$_7$	34.3	8 ± 2	18 ± 3
FN-III$_8$	33.6	8 ± 2	20 ± 3
FN-III$_9$	35.0	9 ± 2	20 ± 3
FN-III$_{10}$	32.1	12 ± 2	22 ± 3

Variability of the midpoints is obtained from analysis of trajectories.

Forced unfolding was accomplished through cf-SMD and cv-SMD protocols. In cf-SMD, unfolding is accomplished by fixing the C_α atom of the N terminus and applying a constant force to the C_α atom of the C terminus along the direction of the vector connecting the two termini (28). Control simulations were conducted by pulling on the N terminus and holding the C terminus fixed; here similar unfolding pathways were observed. The cv-SMD protocol was implemented as described elsewhere (9, 19). A total of 42 cf-SMD and cv-SMD simulations encompassing 45 ns were completed for FN-III modules. Each simulation used ≈200 h on a single SGI R10000 processor at 225 MHz per ns of simulation time.

The cf-SMD protocol was applied to single FN-III$_7$, FN-III$_8$, FN-III$_9$, and FN-III$_{10}$ modules at forces ranging from 350 pN to 1,100 pN. Forces were incrementally lowered in steps of 25–50 pN until no significant unfolding (<10 Å) could be observed in a nanosecond time window. End-to-end distances were determined as the magnitude of the vector separating the C_α atom of the C terminus from the C_α atom of the N terminus. The term extension was defined as the difference in end-to-end distance between equilibrated and stretched structures. Initial end-to-end distances are listed in Table 1. Plateaus from cf-SMD were first determined visually through comparison of multiple time-extension plots. Two plateaus (or shoulders in the case of large forces) were consistently present in all simulations. The extension width of the plateau was determined as the difference between the highest, b, and lowest, a, extension observed without stretching the modules beyond the plateau. The duration of time spent in a plateau, defined as the first passage time, was determined as the difference between the times when a module first reached extension a, and first passed extension b. The midpoint of a plateau was defined as $(a + b)/2$. Visualization and some of the required analysis were done by using the program package VMD 1.5 (29).

Results

Forced Unfolding Studies Using SMD. The early stages of the unfolding pathways were probed for the modules FN-III$_7$, FN-III$_8$, FN-III$_9$, and FN-III$_{10}$ by applying constant external forces (cf-SMD). Fig. 2 shows sample recordings of force-induced unfolding for all four modules. Note that the unfolding time at a given force varies considerably among the modules, decreasing as stronger forces are applied. All curves show multiple plateaus and shoulders, implying that the modules become trapped in intermediate states on their passage to unfolding of their tertiary structure. The conformational state of the modules changes little during their passage through plateaus as only small changes in the rms deviation of backbone coordinates were observed (not shown). The two most pronounced plateaus common to all simulations of FN-III modules are found at extensions ranging from 8 to 12 Å and from 18 to 22 Å. The extension difference

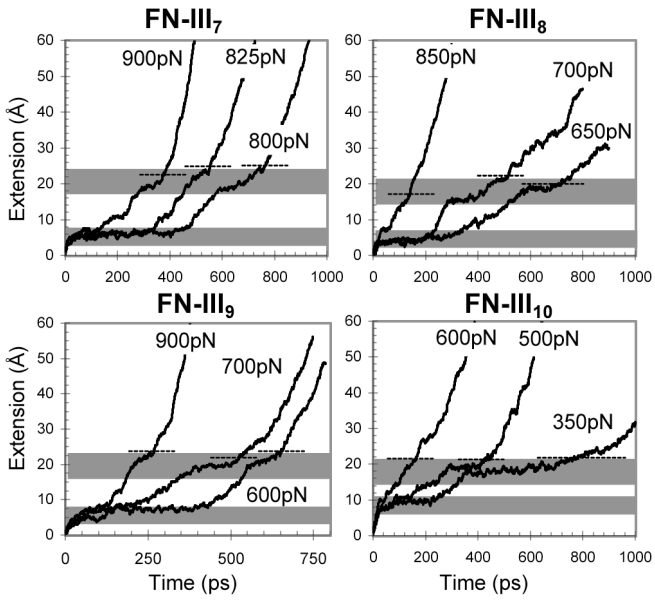

Fig. 2. Representative time extension curves from cf-SMD of FN-III$_7$, FN-III$_8$, FN-III$_9$, and FN-III$_{10}$. At least two plateaus, indicated by shaded boxes, are evident for each simulation. The existence of two plateaus indicates that two major energy barriers have to be crossed before to the first β-strand being broken away. The most common observation in our simulations is that the G-strand is pulled out first, accompanied by the rupture of a cluster of backbone hydrogen bonds connecting the G- and F-strands of the same β-sheet. The extensions at which this rupture occurs are given as dotted lines.

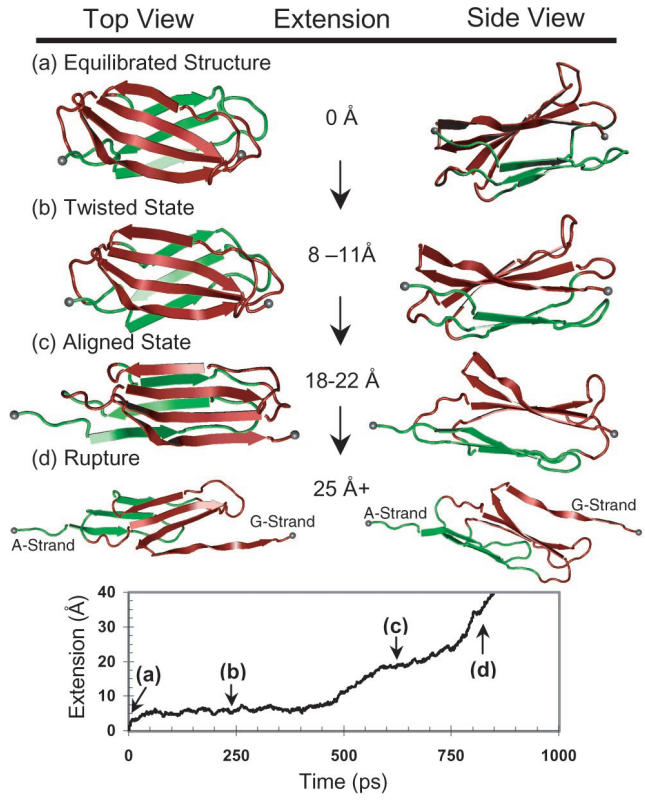

Fig. 3. Sequence of stretching events at extensions smaller than 30 Å. Unfolding proceeds through the following sequence of events: (*a*) equilibrated structure, (*b*) prestretched equilibrated or twisted state, (*c*) intermediate or aligned state, and (*d*) rupture of the cluster of hydrogen bonds between the F- and G-strands. The corresponding time points are indicated in the extension time curve shown below for FN-III$_7$ unfolded at a constant force of 800 pN. Structures were made by using VMD (29).

between the first and second plateau is ≈10 Å for all modules. For each module, small statistical variations exist in the extensions at which the plateaus occur as summarized in Table 1.

As an alternative to cf-SMD, the forced unfolding pathway of FN-III modules can be simulated by pulling their termini apart with cv-SMD as reported (9, 21). Control simulations using cv-SMD also were conducted for each of the modules under otherwise equal conditions. The cv-SMD simulations revealed a primary force peak in the extension/force curves as expected. Closer inspection of the force peaks (not shown) reveals that they are composed of multiple secondary peaks to which little attention has been given previously because of noise inherent to the systems (21). These secondary peaks are also evident in previous studies (9, 21), most notably for FN-III$_7$ where two distinct force peaks are seen in the first 30 Å of unfolding (21). Furthermore, whereas the forces to rupture the FN-III modules depend on the pulling rates (30), the transition states identified by cf-SMD and cv-SMD, and the sequence in which they are passed are essentially the same.

Correlating Plateaus in Extension Time Curves with Conformational Changes. A detailed analysis of all cf-SMD trajectories for modules FN-III$_7$, FN-III$_8$, FN-III$_9$, and FN-III$_{10}$ provides insight into conformational changes that arise at extensions of less than ≈30 Å. As illustrated in Fig. 3, the four FN-III modules have in common that their equilibrated native state becomes prestretched under an external force. This prestretching of the native state does not affect the angle at which the β-strands of the opposing β-sheets are twisted against each other and is thus referred to as the twisted state. The twisted state is associated with the first plateau of the extension time curves shown in Fig. 3*b*. This first plateau is separated by an energy barrier, barrier I, from a second plateau. Mechanical force is required to rotate the two opposing β-sheets of FN-III against each other such that the β-strands of both β-sheets align parallel to the force vector. The state associated with the second plateau is thus defined here as the aligned state. A second energy barrier, barrier II, has to be overcome to break the first major cluster of hydrogen bonds between adjacent β-strands leading to their separation from the main module. The structural hallmarks distinguishing these intermediate states are provided below in more detail.

Starting from the equilibrated native state, the modules extend rapidly by several Å due to the elongation of the randomly coiled terminal residues (twisted state). At the beginning of the first plateau, the modules have a rms deviation of less than 1.0 Å (excluding the terminal residues) from their equilibrated native states. The two opposing β-sheets remain twisted with respect to each other. For the duration of the first plateau, the conformational state remains essentially unperturbed.

The first energy barrier, barrier I, has to be overcome for the modules to extend an additional 10–12 Å from the first to the second plateau. Although essentially all β-strands remain associated with each other through backbone hydrogen bonds, two conserved backbone hydrogen bonds between the A- and B-strands break before extension into the aligned state. These two hydrogen bonds are located immediately following the β-bulge of the A-strand and are highlighted in the sequence alignment in Fig. 1*C*. The straightening of the β-bulge, seen in Fig. 4, is accompanied by backbone torsional rotations in the Φ/ψ angles between the sixth and seventh residues of the A-strand. This seemingly minor structural change creates a gap between the A- and G-strands that is sufficient for 1–3 water molecules to penetrate between the opposing β-sheets. This section of the hydrophobic core (highlighted in the sequence alignment of Fig.

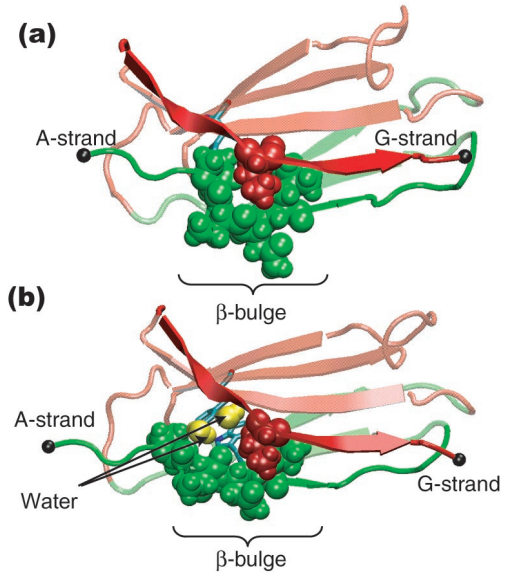

Fig. 4. Shown for FN-III$_7$, structural changes occurring at the end of the first plateau. Breakage of hydrogen bonds highlighted in Fig. 1*C* is immediately followed by straightening of the β-bulge. Atoms of the β-bulge of the A-strand are shown as green spheres. Atoms in red represent the interlocking Ile^{87} residue from the G-strand also specified in Fig. 1*C*. Straightening of the β-bulge creates a gap sufficient for 1–3 waters, shown in yellow, to solvate part of the hydrophobic core that includes Tyr^{34} and Trp^{23}. After these events at extensions (*a*) 7 Å and (*b*) 9 Å, the module extends to the aligned state.

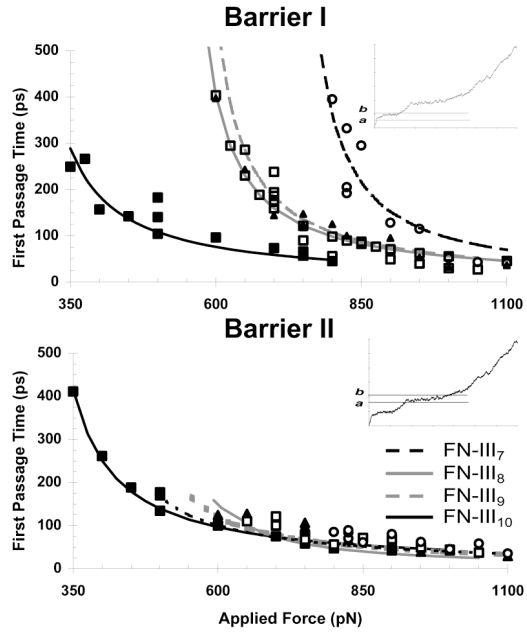

Fig. 5. First passage times vs. applied force for barrier I separating the twisted to aligned state show qualitative differences in first passage times, with ordering FN-III$_7$ > FN-III$_9$ ≈ FN-III$_8$ > FN-III$_{10}$. In contrast, first passage times are approximately equivalent for barrier II separating the aligned state from further unfolding. □, FN-III$_7$; ▲, FN-III$_8$; ◇, FN-III$_9$; ■, FN-III$_{10}$.

1*C* and schematically represented in Fig. 4) consists of a leucine/isoleucine from the G-strand, a proline from the A-strand, tryptophan from the B-strand, and a tyrosine/phenylalanine from the C-strand. This highly conserved tryptophan is shielded from water in the native state of FN-III modules. Its partial solvation was observed in all simulations only when the four FN-III modules were mechanically stretched from the twisted to the aligned state.

Unique to FN-III$_7$, an additional hydrogen bond between the side chain of Tyr^{34}O$^{\eta}$ and the backbone hydrogen of Ser^{26}HN was shown to consistently break before the transition to the aligned state. This hydrogen bond is significant because it is part of the previously mentioned hydrophobic core, and it mechanically connects the upper and lower β-sheets. This hydrogen bond exists only in FN-III$_7$, as FN-III$_8$, FN-III$_9$, and FN-III$_{10}$ possess a proline in place of a serine, thus lacking the essential amine hydrogen necessary for hydrogen bond formation. The function of the hydrogen bond in FN-III$_7$ is considered further in *Discussion*.

After the rupture of these key hydrogen bonds and partial solvation of the hydrophobic core, the β-strands of the two opposing β-sheets rapidly become sheared against each other such that their β-strands align along the direction of the external force as shown in Fig. 3*c*. Rotation of the β-sheets against each other causes significant disruptions in the loops connecting the two β-sheets, including loops BC, DE, and EF (Fig. 1). Once the β-strands are aligned, the modules remain trapped in this aligned state for the duration of the second major plateau, with only slight extension resulting from further shearing between the two β-sheets. The change in the rms deviation from the native to the aligned state is 5 ± 1 Å.

Energy barrier II has to be overcome for the first β-strand(s) to be separated from the main module. Rupture of the FN-III motif begins when the first cluster of backbone hydrogen bonds between neighboring β-strands is broken and the first β-strand separates from the rest of the module (9, 28). Most commonly, the G-strand separated first in our simulations although occasionally, the A- and G-strands separated simultaneously. Rupture continues through several intermediate states that involve the sequential separation of the A-, B-, and F-strands (unpublished work).

Analysis of First Passage Times and Energy Barriers. The duration for which the modules are trapped in a transition state, seen as plateaus in the time extension curves of Fig. 2, provides a measure for the height of the energy barrier that has to be crossed under the influence of stretching and thermal agitation. This duration is defined according to previous work (31, 32) as the first passage time τ. Fig. 5 shows how the first passage times τ to cross barriers I and II depend on the externally applied force. Comparing the four FN-III modules, the force dependency of τ to cross barrier I varies greatly: strongest forces are required for FN-III$_7$ and the weakest for FN-III$_{10}$. The first passage times of barrier II, however, are comparable within our experimental error.

To estimate the height and width of barriers I and II from the monitored first passage times and corresponding extensions, we resort to solving the Smoluchowski equation. The Smoluchowski equation provides an analytical solution if we approximate the barriers by a simple saw-tooth potential: $U(x) = \Delta U(x - a)/(a - b)$ for $a \leq x \leq b$, where ΔU is the height of the potential barrier between extensions a and b (31, 32). Because the modules slightly extend while passing through plateaus, we define the extensions a and b at the beginning and the end of the plateaus, respectively. In this case the mean first passage time, $<\tau>$, is

$$\langle \tau(F) \rangle = 2\tau_d \delta(F)^{-2}[e^{\delta(F)} - \delta(F) - 1], \qquad [1]$$

where F is the externally applied force, $\tau_d = (b - a)^2/2D$, $\delta(F) = \beta[\Delta U - F(b - a)]$, $\beta = 1/k_bT$, and D is the effective diffusion coefficient. A least-square fit of Eq. **1** solving for the two unknown parameters, ΔU and D, was conducted for each of the FN-III modules, using $b - a = 3$ Å and $b - a = 4$ Å for barrier

I and II, respectively. The solution for each of the modules fitted to the τ values obtained for different force values (F) is shown in Fig. 5 together with the original data points. The barriers I separating the twisted from the aligned state varied greatly among modules and were found to be almost 3-fold higher for FN-III$_7$ than for FN-III$_{10}$. The heights for this barrier were 31 $\pm$ 5 kcal/mol for FN-III$_7$, 25 $\pm$ 4 kcal/mol for FN-III$_8$, 24 $\pm$ 4 kcal/mol for FN-III$_9$, and 11 $\pm$ 3 kcal/mol for FN-III$_{10}$. Barrier II heights were similar for the four FN-III modules, being 18 $\pm$ 3, 20 $\pm$ 3, 20 $\pm$ 3, and 22 $\pm$ 3 kcal/mol for FN-III$_7$, FN-III$_8$, FN-III$_9$, and FN-III$_{10}$, respectively. Unfortunately, longer sampling for the second barrier could not be achieved for FN-III$_7$, FN-III$_8$, and FN-III$_9$ because the larger height of barrier II strained computational resources. Although the energy barriers deduced from SMD have the right order of magnitude, their absolute values should be taken with caution because they depend on the assumptions made regarding the shape of the potential. Our simulations, however, should yield a good comparison of the relative heights of barriers I (three times higher for FN-III$_7$ than for FN-III$_{10}$) and barriers II (about equal for the four modules). SMD shows that the barrier crossings comparing different FN-III modules are accompanied by essentially the same structural changes, and extension time plots show their relative width to be the same. A relative comparison of the heights of barrier I and II is more prone to depend on the assumptions made.

Discussion

Studies of early events in the forced unfolding pathway of modules FN-III$_7$, FN-III$_8$, FN-III$_9$, and FN-III$_{10}$ reveal that two energy barriers have to be overcome to extend the modules from their native structure to breaking away the first β-strand(s) defined as the first major rupture. The native state of all FN-III modules consists of two opposing β-sheets that are twisted with respect to each other (twisted state). A first energy barrier, barrier I, separates this twisted from an intermediate state in which the two β-sheets have been sheared against each other with their β-strands coming into alignment (aligned state). A second energy barrier, barrier II, separates this aligned state from rupture of the G-strand.

We also found significant differences in the response of the four FN-III modules to external forces. The heights of barrier I, separating the native state from the aligned state, varied significantly between modules, being largest for FN-III$_7$ and smallest for FN-III$_{10}$, with FN-III$_8$ and FN-III$_9$ falling in between. Conversely the height of barrier II, separating the aligned and ruptured state, was found to be similar for all FN-III modules, suggesting that barrier II is little affected by structural differences among modules. In modular proteins, our cf-SMD data suggest that FN-III$_{10}$ will be one of the first FN-III modules to rupture unless cooperative effects lead to a relative stabilization of neighboring modules.

Structurally, extension from the twisted to aligned states for all FN-III modules investigated here correlates to straightening of a conserved β-bulge and solvation of the peripheral part of the hydrophobic core that includes a highly conserved tryptophan. The breakage of the first two hydrogen bonds between the A- and B-strands following the β-bulge of the A-strand was found to consistently coincide with this event. In simulations where the partial charges of just these two hydrogen bonds were set to zero and simulations were restarted from the original equilibrated structures, the first passage times for these simulations were found to decrease approximately by one-half for barrier I. In these simulations, the G-strand continued to peel away first, despite the fact that hydrogen bonds between the A- and B-strands were removed. In addition, no significant reduction in first passage time was seen when the partial charges of the last two hydrogen bonds between the F- and G-strands were removed.

Our results further suggest that the enhanced stability seen for FN-III$_7$ is due to a tyrosine hydrogen bond formed between Tyr^{34}O$^{\eta}$ and the backbone hydrogen of Lys^{29}-HN, which effectively crosslinks the β-sheets. Removal of this hydrogen bond resulted in a reduction of the first passage time from 500 ps to 100 ps at a force of 800 pN, in line with the passage times found for FN-III$_8$ and FN-III$_9$ when the same force was applied. Although we were not able to directly determine why barrier I is lowest for FN-III$_{10}$, we speculate that substitution of a hydrophilic Arg^6 weakens hydrogen bonding between the A-and B-strands.

Existence of an intermediate state in the unfolding and folding pathways of FN-III modules also has been noted in recent kinetic studies where single FN-III modules were denatured chemically (33) or thermally (34). Here we describe an intermediate state in the forced unfolding pathway of FN-III modules, referred to as the aligned state. Future work has to reveal whether the intermediate state found in protein folding kinetics is the same as the one found along the forced unfolding pathway.

Although no experimental data are available on the relative mechanical stability of FN-III modules, several denaturant and thermal unfolding studies have investigated the stabilities of FN-III$_9$ and FN-III$_{10}$. These studies have shown that the free energy difference between the completely unfolded and native state is considerably higher for FN-III$_{10}$ than for FN-III$_9$ (33–35). However, these data do not contradict our simulations that reveal a higher mechanical stability for FN-III$_9$ than for FN-III$_{10}$, because forced unfolding is a kinetic process that probes barrier heights rather than equilibrium energies. AFM studies of the unfolding and refolding kinetics of single I-27 modules showed that the rate constants obtained in stretching experiments compared closely to rates derived from unfolding and refolding kinetics of chemically denatured I-27 modules (36). When comparing the relative stabilities of I-27 and I-28, the free energy difference between the ruptured and native state is considerably higher for I-27 than for I-28, whereas the energy barrier separating those two states is higher for I-28 than for I-27. Consequently, it was found that I-27 is thermodynamically more stable than I-28, while I-28 is mechanically more stable than I-27 (18). Unfortunately, the free energy differences between the native and intermediate states have not yet been determined for any FN-III module, most likely due to the short-lived nature (33, 34) of the intermediate state. Although FN-III$_9$ is thermodynamically less stable than FN-III$_{10}$, our SMD data suggest that FN-III$_9$ is mechanically more stable than FN-III$_{10}$.

Simulations using simplifying assumptions to reduce the size of the system predicted that FN-III$_9$ is mechanically less stable than FN-III$_{10}$ (22, 23, 37). The simulations by Paci and Karplus (22, 23), for example, used an implicit solvent description including only polar hydrogens and suggested that electrostatic interactions do not contribute to the mechanical stability of FN-III modules. Although the experimental answer regarding their relative stability remains open, the importance of backbone hydrogen bonds with a similar β-sandwich motif, I27, recently has been demonstrated by AFM using I27 mutants (37). Previous SMD suggests that water plays an important role in Ig stretching by competing for backbone hydrogen bonds (38).

One of the reasons nature has chosen to build FN from more than 15 different FN-III building blocks may be that all of the modules vary in energy barrier heights between intermediate and unfolded states. This built-in difference in mechanical stability would not only allow fine-tuning of the elastic response, but it would define precisely which modules prestretch or rupture for a given external force. Fine-tuning of the mechanical stability of the FN-III modules occurs through structural changes affecting mainly barrier I.

Prestretching and transitioning into an intermediate state will alter the distance between neighboring modules, thereby potentially exposing otherwise cryptic binding sites. The midpoints of the aligned state are found for all modules at an extension of 20 Å (or ≈10 Å extended from the twisted state). Cryptic sites have been specifically proposed to exist in FN-III$_1$, FN-III$_{7–8}$, and FN-III$_{10}$ (11). Although our SMD simulations suggest that FN-III$_7$ is relatively stable, the cryptic site in the FN-III$_{7–8}$ dimer could be located at the interface between the two modules (12), implying that prestretching of FN-III$_8$ into the aligned state exposes the interface between the modules. Other researchers have suggested that FN-III$_{10}$ contains a cryptic site that binds to FN-III$_1$ when FN-III$_{10}$ is denatured (7, 39). Our finding of a mechanically less stable FN-III$_{10}$ suggests that fine-tuning of the energy barrier height between the native and the intermediate (aligned) state of FN-III modules may play a significant regulatory role. In FN fibril assembly, for example, the applied force may control the sequence in which cryptic sites become exposed.

The finding that FN-III$_{10}$ is the mechanically least stable of the four modules studied also may be important in light of earlier predictions that the FN-III$_{10}$ module is designed to act as a force-regulated molecular recognition switch (9). It is proposed that the RGD loop connecting the F- and G-strands is shortened immediately after the breaking away of the first β-strand (9). The G-strand is observed most frequently by SMD to be separated first whereas the remaining module essentially maintains its structural integrity early after this rupture. Shortening of the RGD loop below 10 Å has been shown experimentally to reduce the accessibility of the RGD loop to integrins (40). Unless FN-III$_{10}$ is mechanically more stabilized than the other modules within FN fibers, the simulations reported in this article would predict that access to the RGD site would be reduced in early stages of stretching FN fibers, assuming that the FN fiber elasticity originates from the unfolding of individual FN modules.

In conclusion, SMD simulations of the forced-unfolding pathway of the FN-III modules gives intriguing insight into the relative mechanical stability of FN-III modules. These studies also illustrate how nature may use force to regulate the exposure of recognition sites by tightly controlling which of the modules is first extended into the intermediate state and which will rupture first. Point mutations to the FN-III modules can have a pronounced impact on the energy barrier separating the native and intermediate state.

We thank Meher Antia, Gretchen Baneyx, Hui Lu, Terry Lybrand, John Saeger, and Wendy Thomas for fruitful discussions. We acknowledge support from National Institutes of Health grants (R01 GM49063–07, R01 GM60946–01, NIH 5 T32 GM08268). Software and computer resources were provided by the National Center for Research Resources. Resource for Biomolecular Modeling (NIH PHS 5 P41 RR05969) and by a National Science Foundation computer time grant (MCA93S028).

1. Ohashi, T., Kiehart, D. P. & Erickson, H. P. (1999) *Proc. Natl. Acad. Sci. USA* **96,** 2153–2158.
2. Hynes, R. O. (1999) *Proc. Natl. Acad. Sci. USA* **96,** 2588–2590.
3. Erickson, H. P. (1994) *Proc. Natl. Acad. Sci. USA* **91,** 10114–10118.
4. Leahy, D. J., Aukhil, I. & Erickson, H. P. (1996) *Cell* **84,** 155–164.
5. Hynes, R. O. (1990) *Fibronectins* (Springer, New York).
6. Richardson, J. S. (1977) *Nature (London)* **268,** 495–500.
7. Zhong, C., Chrzanowska-Wodnicka, M., Brown, J., Shaub, A., Belkin, A. M. & Burridge, K. (1998) *J. Cell Biol.* **141,** 539–551.
8. Hocking, D. C., Smith, R. K. & McKeown-Longo, P. J. (1996) *J. Cell Biol.* **133,** 431–444.
9. Krammer, A., Lu, H., Isralewitz, B., Schulten, K. & Vogel, V. (1999) *Proc. Natl. Acad. Sci. USA* **96,** 1351–1356.
10. Baneyx, G. & Vogel, V. (1999) *Proc. Natl. Acad. Sci. USA* **96,** 12518–12523.
11. Litvinovich, S. V. & Ingham, K. C. (1995) *J. Mol. Biol.* **248,** 611–626.
12. Ingham, K. C., Brew, S. A., Huff, S. & Litvinovich, S. V. (1997) *J. Biol. Chem.* **272,** 1718–1724.
13. Oberhauser, A. F., Marszalek, P. E., Erickson, H. P. & Fernandez, J. M. (1998) *Nature (London)* **393,** 181–185.
14. Rief, M., Gautel, M. & Gaub, H. E. (2000) *Adv. Exp. Med. Biol.* **481,** 129–136.
15. Oberdorfer, Y. F., Fuchs, H. & Janshoff, A. (2000) *Langmuir* **16,** 9955–9958.
16. Kellermayer, M. S., Smith, S. B., Granzier, H. L. & Bustamante, C. (1997) *Science* **276,** 1112–1116.
17. Rief, M., Gautel, M., Schemmel, A. & Gaub, H. E. (1998) *Biophys. J.* **75,** 3008–3014.
18. Li, H., Oberhauser, A. F., Fowler, S. B., Clarke, J. & Fernandez, J. M. (2000) *Proc. Natl. Acad. Sci. USA* **97,** 6527–6531. (First Published May 23, 2000, 10.1073/pnas.120048697)
19. Lu, H., Isralewitz, B., Krammer, A., Vogel, V. & Schulten, K. (1998) *Biophys. J.* **75,** 662–671.
20. Marszalek, P. E., Lu, H., Li, H., Carrion-Vazquez, M., Oberhauser, A. F., Schulten, K. & Fernandez, J. M. (1999) *Nature (London)* **402,** 100–103.
21. Lu, H. & Schulten, K. (1999) *Proteins* **35,** 453–463.
22. Paci, E. & Karplus, M. (1999) *J. Mol. Biol.* **288,** 441–459.
23. Paci, E. & Karplus, M. (2000) *Proc. Natl. Acad. Sci. USA* **97,** 6521–6526. (First Published May 23, 2000, 10.1073/pnas.100124597)
24. MacKerell, A. D., Bashford, D., Bellot, M., Dunbrack, R. L., Jr., Evansec, J., Field, M. J., Fischer, S., Gao, J., Guo, H., Ha, S., *et al.* (1998) *J. Phys. Chem. B* **102,** 3586–3616.
25. Jorgensen, W. L., Chandrasekhar, J., Madura, J. D., Impey, R. W. & Klein, M. L. (1983) *J. Chem. Phys.* **79,** 926–935.
26. Nelson, M. T., Humphrey, W., Gursoy, A., Dalke, A., Kale, L. V., Skeel, R. D. & Schulten, K. (1996) *Int. J. Supercomput. Appl.* **10,** 251–268.
27. Brunger, A. T. (1992) X-PLOR*: A System for X-Ray Cyrstallography and NMR* (Yale Univ. Press, New Haven, CT).
28. Lu, H. & Schulten, K. (1999) *Chem. Phys.* **247,** 141–153.
29. Humphrey, W., Dalke, A. & Schulten, K. (1996) *J. Mol. Graphics* **14,** 33–38.
30. Evans, E. & Ritchie, K. (1997) *Biophys. J.* **72,** 1541–1555.
31. Izrailev, S., Stepaniants, S., Balsera, M., Oono, Y. & Schulten, K. (1997) *Biophys. J.* **72,** 1568–1581.
32. Balsera, M., Stepaniants, S., Izrailev, S., Oono, Y. & Schulten, K. (1997) *Biophys. J.* **73,** 1281–1287.
33. Cota, E. & Clarke, J. (2000) *Protein Sci.* **9,** 112–120.
34. Litvinovich, S. V., Brew, S. A., Aota, S., Akiyama, S. K., Haudenschild, C. & Ingham, K. C. (1998) *J. Mol. Biol.* **280,** 245–258.
35. Plaxco, K. W., Spitzfaden, C., Campbell, I. D. & Dobson, C. M. (1997) *J. Mol. Biol.* **270,** 763–770.
36. Carrion-Vazquez, M., Oberhauser, A. F., Fowler, S. B., Marszalek, P. E., Broedel, S. E., Clarke, J. & Fernandez, J. M. (1999) *Proc. Natl. Acad. Sci. USA* **96,** 3694–3699.
37. Li, H., Carrion-Vazquez, M., Oberhauser, A. F., Marszalek, P. E. & Fernandez, J. M. (2000) *Nat. Struct. Biol.* **7,** 1117–1120.
38. Lu, H. & Schulten, K. (2000) *Biophys. J.* **79,** 51–65.
39. Hocking, D. C., Sottile, J. & McKeown-Longo, P. J. (1998) *J. Cell Biol.* **141,** 241–253.
40. Spitzfaden, C., Grant, R. P., Mardon, H. J. & Campbell, I. D. (1997) *J. Mol. Biol.* **265,** 565–579.